

Observation of radiative $B^0 \rightarrow \phi K^0 \gamma$ decays

I. Adachi,¹⁰ H. Aihara,⁵⁹ K. Arinstein,^{1,41} T. Aso,⁶³ V. Aulchenko,^{1,41} T. Aushev,^{26,19}
T. Aziz,⁵⁴ S. Bahinipati,³ A. M. Bakich,⁵³ V. Balagura,¹⁹ Y. Ban,⁴⁵ E. Barberio,³⁰
A. Bay,²⁶ I. Bedny,^{1,41} K. Belous,¹⁶ V. Bhardwaj,⁴⁴ B. Bhuyan,¹³ M. Bischofberger,³³
S. Blyth,³⁵ A. Bondar,^{1,41} A. Bozek,³⁷ M. Bračko,^{28,20} J. Brodzicka,³⁷ T. E. Browder,⁹
M.-C. Chang,⁴ P. Chang,³⁶ Y.-W. Chang,³⁶ Y. Chao,³⁶ A. Chen,³⁴ K.-F. Chen,³⁶
P.-Y. Chen,³⁶ B. G. Cheon,⁸ C.-C. Chiang,³⁶ R. Chistov,¹⁹ I.-S. Cho,⁶⁵ S.-K. Choi,⁷
Y. Choi,⁵² J. Crnkovic,¹² J. Dalseno,^{29,55} M. Danilov,¹⁹ A. Das,⁵⁴ M. Dash,⁶⁴
A. Drutskoy,³ W. Dungel,¹⁵ S. Eidelman,^{1,41} D. Epifanov,^{1,41} M. Feindt,²² H. Fujii,¹⁰
M. Fujikawa,³³ N. Gabyshev,^{1,41} A. Garmash,^{1,41} G. Gokhroo,⁵⁴ P. Goldenzweig,³
B. Golob,^{27,20} M. Grosse Perdekamp,^{12,47} H. Guo,⁴⁹ H. Ha,²³ J. Haba,¹⁰ B.-Y. Han,²³
K. Hara,³¹ T. Hara,¹⁰ Y. Hasegawa,⁵¹ N. C. Hastings,⁵⁹ K. Hayasaka,³¹ H. Hayashii,³³
M. Hazumi,¹⁰ D. Heffernan,⁴³ T. Higuchi,¹⁰ Y. Horii,⁵⁸ Y. Hoshi,⁵⁷ K. Hoshina,⁶²
W.-S. Hou,³⁶ Y. B. Hsiung,³⁶ H. J. Hyun,²⁵ Y. Igarashi,¹⁰ T. Iijima,³¹ K. Inami,³¹
A. Ishikawa,⁴⁸ H. Ishino,^{60,*} K. Itoh,⁵⁹ R. Itoh,¹⁰ M. Iwabuchi,⁶ M. Iwasaki,⁵⁹ Y. Iwasaki,¹⁰
T. Jinno,³¹ M. Jones,⁹ N. J. Joshi,⁵⁴ T. Julius,³⁰ D. H. Kah,²⁵ H. Kakuno,⁵⁹ J. H. Kang,⁶⁵
P. Kapusta,³⁷ S. U. Kataoka,³² N. Katayama,¹⁰ H. Kawai,² T. Kawasaki,³⁹ A. Kibayashi,¹⁰
H. Kichimi,¹⁰ C. Kiesling,²⁹ H. J. Kim,²⁵ H. O. Kim,²⁵ J. H. Kim,⁵² S. K. Kim,⁵⁰
Y. I. Kim,²⁵ Y. J. Kim,⁶ K. Kinoshita,³ B. R. Ko,²³ S. Korpar,^{28,20} M. Kreps,²²
P. Križan,^{27,20} P. Krokovny,¹⁰ T. Kuhr,²² R. Kumar,⁴⁴ T. Kumita,⁶¹ E. Kurihara,²
E. Kuroda,⁶¹ Y. Kuroki,⁴³ A. Kusaka,⁵⁹ A. Kuzmin,^{1,41} Y.-J. Kwon,⁶⁵ S.-H. Kyeong,⁶⁵
J. S. Lange,⁵ G. Leder,¹⁵ M. J. Lee,⁵⁰ S. E. Lee,⁵⁰ S.-H. Lee,²³ J. Li,⁹ A. Limosani,³⁰
S.-W. Lin,³⁶ C. Liu,⁴⁹ D. Liventsev,¹⁹ R. Louvot,²⁶ J. MacNaughton,¹⁰ F. Mandl,¹⁵
D. Marlow,⁴⁶ A. Matyja,³⁷ S. McOnie,⁵³ T. Medvedeva,¹⁹ Y. Mikami,⁵⁸ K. Miyabayashi,³³
H. Miyake,⁴³ H. Miyata,³⁹ Y. Miyazaki,³¹ R. Mizuk,¹⁹ A. Moll,^{29,55} T. Mori,³¹ T. Müller,²²
R. Mussa,¹⁸ T. Nagamine,⁵⁸ Y. Nagasaka,¹¹ Y. Nakahama,⁵⁹ I. Nakamura,¹⁰ E. Nakano,⁴²
M. Nakao,¹⁰ H. Nakayama,⁵⁹ H. Nakazawa,³⁴ Z. Natkaniec,³⁷ K. Neichi,⁵⁷ S. Neubauer,²²
S. Nishida,¹⁰ K. Nishimura,⁹ O. Nitoh,⁶² S. Noguchi,³³ T. Nozaki,¹⁰ A. Ogawa,⁴⁷
S. Ogawa,⁵⁶ T. Ohshima,³¹ S. Okuno,²¹ S. L. Olsen,⁵⁰ W. Ostrowicz,³⁷ H. Ozaki,¹⁰
P. Pakhlov,¹⁹ G. Pakhlova,¹⁹ H. Palka,³⁷ C. W. Park,⁵² H. Park,²⁵ H. K. Park,²⁵
K. S. Park,⁵² L. S. Peak,⁵³ M. Pernicka,¹⁵ R. Pestotnik,²⁰ M. Peters,⁹ L. E. Piilonen,⁶⁴
A. Poluektov,^{1,41} K. Prothmann,^{29,55} B. Riesert,²⁹ M. Rozanska,³⁷ H. Sahoo,⁹
K. Sakai,³⁹ Y. Sakai,¹⁰ N. Sasao,²⁴ O. Schneider,²⁶ P. Schönmeier,⁵⁸ J. Schümann,¹⁰
C. Schwanda,¹⁵ A. J. Schwartz,³ R. Seidl,⁴⁷ A. Sekiya,³³ K. Senyo,³¹ M. E. Sevier,³⁰
L. Shang,¹⁴ M. Shapkin,¹⁶ V. Shebalin,^{1,41} C. P. Shen,⁹ H. Shibuya,⁵⁶ S. Shiizuka,³¹
S. Shinomiya,⁴³ J.-G. Shiu,³⁶ B. Shwartz,^{1,41} F. Simon,^{29,55} J. B. Singh,⁴⁴ R. Sinha,¹⁷
A. Sokolov,¹⁶ E. Solovieva,¹⁹ S. Stanič,⁴⁰ M. Starič,²⁰ J. Stypula,³⁷ A. Sugiyama,⁴⁸
K. Sumisawa,¹⁰ T. Sumiyoshi,⁶¹ S. Suzuki,⁴⁸ S. Y. Suzuki,¹⁰ Y. Suzuki,³¹ F. Takasaki,¹⁰
N. Tamura,³⁹ K. Tanabe,⁵⁹ M. Tanaka,¹⁰ N. Taniguchi,¹⁰ G. N. Taylor,³⁰ Y. Teramoto,⁴²
I. Tikhomirov,¹⁹ K. Trabelsi,¹⁰ Y. F. Tse,³⁰ T. Tsuboyama,¹⁰ K. Tsunada,³¹ Y. Uchida,⁶
S. Uehara,¹⁰ Y. Ueki,⁶¹ K. Ueno,³⁶ T. Uglov,¹⁹ Y. Unno,⁸ S. Uno,¹⁰ P. Urquijo,³⁰
Y. Ushiroda,¹⁰ Y. Usov,^{1,41} G. Varner,⁹ K. E. Varvell,⁵³ K. Vervink,²⁶ A. Vinokurova,^{1,41}
C. C. Wang,³⁶ C. H. Wang,³⁵ J. Wang,⁴⁵ M.-Z. Wang,³⁶ P. Wang,¹⁴ X. L. Wang,¹⁴

M. Watanabe,³⁹ Y. Watanabe,²¹ R. Wedd,³⁰ J.-T. Wei,³⁶ J. Wicht,¹⁰ L. Widhalm,¹⁵
J. Wiechczynski,³⁷ E. Won,²³ B. D. Yabsley,⁵³ H. Yamamoto,⁵⁸ Y. Yamashita,³⁸
M. Yamauchi,¹⁰ C. Z. Yuan,¹⁴ Y. Yusa,⁶⁴ C. C. Zhang,¹⁴ L. M. Zhang,⁴⁹ Z. P. Zhang,⁴⁹
V. Zhilich,^{1,41} V. Zhulanov,^{1,41} T. Zivko,²⁰ A. Zupanc,²⁰ N. Zwahlen,²⁶ and O. Zyukova^{1,41}

(The Belle Collaboration)

¹*Budker Institute of Nuclear Physics, Novosibirsk*

²*Chiba University, Chiba*

³*University of Cincinnati, Cincinnati, Ohio 45221*

⁴*Department of Physics, Fu Jen Catholic University, Taipei*

⁵*Justus-Liebig-Universität Gießen, Gießen*

⁶*The Graduate University for Advanced Studies, Hayama*

⁷*Gyeongsang National University, Chinju*

⁸*Hanyang University, Seoul*

⁹*University of Hawaii, Honolulu, Hawaii 96822*

¹⁰*High Energy Accelerator Research Organization (KEK), Tsukuba*

¹¹*Hiroshima Institute of Technology, Hiroshima*

¹²*University of Illinois at Urbana-Champaign, Urbana, Illinois 61801*

¹³*India Institute of Technology Guwahati, Guwahati*

¹⁴*Institute of High Energy Physics,*

Chinese Academy of Sciences, Beijing

¹⁵*Institute of High Energy Physics, Vienna*

¹⁶*Institute of High Energy Physics, Protvino*

¹⁷*Institute of Mathematical Sciences, Chennai*

¹⁸*INFN - Sezione di Torino, Torino*

¹⁹*Institute for Theoretical and Experimental Physics, Moscow*

²⁰*J. Stefan Institute, Ljubljana*

²¹*Kanagawa University, Yokohama*

²²*Institut für Experimentelle Kernphysik, Universität Karlsruhe, Karlsruhe*

²³*Korea University, Seoul*

²⁴*Kyoto University, Kyoto*

²⁵*Kyungpook National University, Taegu*

²⁶*École Polytechnique Fédérale de Lausanne (EPFL), Lausanne*

²⁷*Faculty of Mathematics and Physics, University of Ljubljana, Ljubljana*

²⁸*University of Maribor, Maribor*

²⁹*Max-Planck-Institut für Physik, München*

³⁰*University of Melbourne, School of Physics, Victoria 3010*

³¹*Nagoya University, Nagoya*

³²*Nara University of Education, Nara*

³³*Nara Women's University, Nara*

³⁴*National Central University, Chung-li*

³⁵*National United University, Miao Li*

³⁶*Department of Physics, National Taiwan University, Taipei*

³⁷*H. Niewodniczanski Institute of Nuclear Physics, Krakow*

³⁸*Nippon Dental University, Niigata*

³⁹*Niigata University, Niigata*

⁴⁰*University of Nova Gorica, Nova Gorica*

- ⁴¹*Novosibirsk State University, Novosibirsk*
⁴²*Osaka City University, Osaka*
⁴³*Osaka University, Osaka*
⁴⁴*Panjab University, Chandigarh*
⁴⁵*Peking University, Beijing*
⁴⁶*Princeton University, Princeton, New Jersey 08544*
⁴⁷*RIKEN BNL Research Center, Upton, New York 11973*
⁴⁸*Saga University, Saga*
⁴⁹*University of Science and Technology of China, Hefei*
⁵⁰*Seoul National University, Seoul*
⁵¹*Shinshu University, Nagano*
⁵²*Sungkyunkwan University, Suwon*
⁵³*School of Physics, University of Sydney, NSW 2006*
⁵⁴*Tata Institute of Fundamental Research, Mumbai*
⁵⁵*Excellence Cluster Universe, Technische Universität München, Garching*
⁵⁶*Toho University, Funabashi*
⁵⁷*Tohoku Gakuin University, Tagajo*
⁵⁸*Tohoku University, Sendai*
⁵⁹*Department of Physics, University of Tokyo, Tokyo*
⁶⁰*Tokyo Institute of Technology, Tokyo*
⁶¹*Tokyo Metropolitan University, Tokyo*
⁶²*Tokyo University of Agriculture and Technology, Tokyo*
⁶³*Toyama National College of Maritime Technology, Toyama*
⁶⁴*IPNAS, Virginia Polytechnic Institute and State University, Blacksburg, Virginia 24061*
⁶⁵*Yonsei University, Seoul*

Abstract

We report the first observation of radiative decay $B^0 \rightarrow \phi K^0 \gamma$ using a data sample of 772×10^6 $B\bar{B}$ pairs collected at the $\Upsilon(4S)$ resonance with the Belle detector at the KEKB asymmetric-energy e^+e^- collider. We observe a signal of 35 ± 8 events with a significance of 5.4 standard deviations including systematic uncertainties. The measured branching fraction is $\mathcal{B}(B^0 \rightarrow \phi K^0 \gamma) = (2.66 \pm 0.60 \pm 0.32) \times 10^{-6}$. We also precisely measure $\mathcal{B}(B^+ \rightarrow \phi K^+ \gamma) = (2.34 \pm 0.29 \pm 0.23) \times 10^{-6}$. The uncertainties are statistical and systematic, respectively. The observed $M_{\phi K}$ mass spectrum differs significantly from that expected in a three-body phase-space decay.

PACS numbers: 14.40.Nd, 13.25.Hw, 11.30.Er

Rare radiative decays of B mesons play an important role in the search for physics beyond the standard model (SM) of electroweak interactions. These flavor changing neutral current decays are forbidden at tree level in the SM, but allowed through electroweak loop processes. The loop can be mediated by non-SM particles (for example, charged Higgs or SUSY particles), which could affect either the branching fraction or the time-dependent CP asymmetry.

The current measured inclusive world average branching fraction for $B \rightarrow X_s \gamma$ ($(3.55 \pm 0.26) \times 10^{-4}$ [1]), is one standard deviation (σ) higher than the SM prediction at next-to-next-to-leading order (NNLO) $(3.15 \pm 0.23) \times 10^{-4}$ [2], and still allows significant new physics contributions to radiative B decays. Exclusive $b \rightarrow s \gamma$ decays have also been extensively measured, but their sum so far accounts only for 44% of the inclusive rate. Therefore, further measurements of branching fractions for exclusive $B \rightarrow \phi K \gamma$ modes will improve our understanding of the $b \rightarrow s \gamma$ process. The neutral mode $B^0 \rightarrow \phi K^0 \gamma$ [3] can be used to study time-dependent CP asymmetry, which is suppressed in the SM by the quark mass ratio ($2m_s/m_b$) [4, 5]. In several models beyond SM, the photon acquires an appreciable right-handed component due to the exchange of a virtual heavy fermion in the loop process, resulting in large values of time-dependent CP asymmetries. Due to the narrow width of the ϕ resonance, the decay $B \rightarrow \phi K \gamma$ is well separated from the background and can be effectively used for measurements of photon momentum over a wide interval. In addition, this mode can also be used to search for a possible contribution from kaonic resonances decaying to ϕK . Furthermore, we can probe the photon polarization using the angular distributions of the final state hadrons [6, 7].

The decay $B^0 \rightarrow \phi K_S^0 \gamma$ can be described by the conventional radiative penguin diagram with the creation of an additional $s\bar{s}$ pair as shown in Fig. 1.

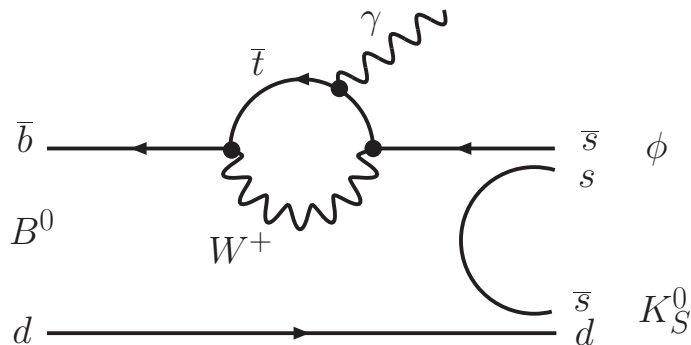


FIG. 1: Feynman diagram for the radiative penguin decay $B^0 \rightarrow \phi K_S^0 \gamma$ with $s\bar{s}$ pair creation.

The branching fractions for $B \rightarrow \phi K \gamma$ decays have already been reported by the Belle and BaBar collaborations. Belle measured $\mathcal{B}(B^+ \rightarrow \phi K^+ \gamma) = (3.4 \pm 0.9 \pm 0.4) \times 10^{-6}$ and $\mathcal{B}(B^0 \rightarrow \phi K^0 \gamma) < 8.3 \times 10^{-6}$ at the 90% confidence level (C.L.) using $96 \times 10^6 B\bar{B}$ pairs [8]. BaBar measured $\mathcal{B}(B^+ \rightarrow \phi K^+ \gamma) = (3.5 \pm 0.6 \pm 0.4) \times 10^{-6}$ and $\mathcal{B}(B^0 \rightarrow \phi K^0 \gamma) < 2.7 \times 10^{-6}$ at the 90% C.L. using $228 \times 10^6 B\bar{B}$ pairs [9]. BaBar also reported the direct CP asymmetry for $B^\pm \rightarrow \phi K^\pm \gamma$, $\mathcal{A}_{CP} = (-26 \pm 14 \pm 5)\%$. We report herein the first observation of radiative decay $B^0 \rightarrow \phi K^0 \gamma$ and an improved measurement of $B^+ \rightarrow \phi K^+ \gamma$ using a data sample of $772 \times 10^6 B\bar{B}$ pairs collected at the $\Upsilon(4S)$ resonance with the Belle detector at the KEKB asymmetric-energy e^+e^- collider [10]. This data sample is nearly eight times larger than the

sample used in our previous measurement [8].

The Belle detector is a large-solid-angle magnetic spectrometer that consists of a silicon vertex detector (SVD), a 50-layer central drift chamber (CDC), an array of aerogel threshold Cherenkov counters (ACC), a barrel-like arrangement of time-of-flight scintillation counters (TOF), and an electromagnetic calorimeter (ECL) comprised of CsI(Tl) crystals located inside a superconducting solenoid coil that provides a 1.5 T magnetic field. An iron flux-return located outside the coil is instrumented to detect K_L^0 mesons and to identify muons (KLM). The detector is described in detail elsewhere [11]. Two different inner detector configurations were used. For the first sample of 152×10^6 $B\bar{B}$ pairs, a 2.0 cm radius beampipe and a 3-layer silicon vertex detector (SVD-I) were used; for the latter 620×10^6 $B\bar{B}$ pairs, a 1.5 cm radius beampipe, a 4-layer silicon vertex detector (SVD-II), and a small-cell inner drift chamber were used. A GEANT-based simulation of the Belle detector is used to produce signal Monte Carlo (MC) [12] event samples.

The signal is reconstructed in the decays $B^+ \rightarrow \phi K^+ \gamma$ and $B^0 \rightarrow \phi K_S^0 \gamma$, with $\phi \rightarrow K^+ K^-$ and $K_S^0 \rightarrow \pi^+ \pi^-$. All the charged tracks used in the reconstruction (except for charged pions from K_S^0 's) are required to satisfy a requirement on the distance of closest approach to the interaction point (IP) along the beam direction, $|dz| < 5$ cm, and in the transverse direction, $dr < 2$ cm. This eliminates poorly reconstructed tracks or tracks that do not come from the interaction region. Charged kaons are identified using a likelihood ratio $\mathcal{L}(K/\pi) > 0.6$, based on information from the ACC, TOF and CDC (dE/dx) detectors. This requirement has an efficiency of 90% for kaons with a 8% pion fake rate. A less restrictive likelihood ratio requirement $\mathcal{L}(K/\pi) > 0.4$ is applied to the kaon candidates, which are used to reconstruct the ϕ meson. The invariant mass of the ϕ candidates is required to be within $-0.01 \text{ GeV}/c^2 < M_{K^+ K^-} - m_\phi < +0.01 \text{ GeV}/c^2$, where m_ϕ denotes the world-average ϕ mass [13].

Neutral kaon (K_S^0) candidates are formed from the $\pi^+ \pi^-$ combinations with invariant mass in the range $0.482 \text{ GeV}/c^2 < M_{\pi^+ \pi^-} < 0.514 \text{ GeV}/c^2$. The selected candidates must pass a set of momentum-dependent requirements on impact parameter, vertex displacement, mismatch in the z direction, and the direction of the pion pair momentum as described in the Ref. [14].

The primary signature of this decay is a high energy prompt photon. These are selected from isolated ECL clusters within the barrel region ($32^\circ < \theta_\gamma < 129^\circ$, where θ_γ is the polar angle of the photon in the laboratory frame) and center-of-mass system (cms) energy (E_γ^{cms}) in the range 1.4 to 3.4 GeV. The selected photon candidates are required to be consistent with isolated electromagnetic showers, i.e., 95% of the energy in an array of 5×5 CsI(Tl) crystals should be concentrated in an array of 3×3 crystals and should have no charged tracks associated with it. We also suppress the background photons from $\pi^0(\eta) \rightarrow \gamma\gamma$ using a likelihood $\mathcal{L}_{\pi^0}(\mathcal{L}_\eta) < 0.25$, calculated for each photon pair consisting of the candidate photon and any other photon in the event [15].

We combine a ϕ meson candidate, a charged or neutral kaon candidate and the radiative photon to form a B meson. The B candidates are identified using two kinematic variables: the energy difference $\Delta E \equiv E_B^{\text{cms}} - E_{\text{beam}}^{\text{cms}}$ and the beam-energy-constrained mass $M_{\text{bc}} \equiv \sqrt{(E_{\text{beam}}^{\text{cms}})^2 - (p_B^{\text{cms}})^2}$, where $E_{\text{beam}}^{\text{cms}}$ is the beam energy in the cms, and E_B^{cms} and p_B^{cms} are the cms energy and momentum, respectively, of the reconstructed B candidate. In the M_{bc} calculation, the photon momentum is replaced by $(E_{\text{beam}}^{\text{cms}} - E_{\phi K}^{\text{cms}})$ to improve resolution. The events that satisfy the requirements $M_{\text{bc}} > 5.2 \text{ GeV}/c^2$ and $|\Delta E| < 0.3 \text{ GeV}$ (defined as the fit region) are selected for further analysis. Using MC simulations, we find nearly 12%

(3%) of events have more than one B candidate for the $B^+ \rightarrow \phi K^+ \gamma$ ($B^0 \rightarrow \phi K^0 \gamma$) mode. In case of multiple candidates, we choose the best candidate based on a series of selection criteria, which depend on a χ^2 variable using the candidate's ϕ mass (and the K_S^0 mass in the neutral mode) as well as the highest E_γ^{cms} and the highest $\mathcal{L}(K/\pi)$ in the charged mode. For events with multiple candidates, this selection method chooses the correct B candidate for the $B^+ \rightarrow \phi K^+ \gamma$ ($B^0 \rightarrow \phi K^0 \gamma$) mode 57% (69%) of the time. We define the signal region as $5.27 \text{ GeV}/c^2 < M_{\text{bc}} < 5.29 \text{ GeV}/c^2$ and $-0.08 \text{ GeV} < \Delta E < 0.05 \text{ GeV}$. The ΔE signal region is asymmetric in order to include the tail in the lower region due to photon energy leakage in the ECL.

The dominant background comes from $e^+e^- \rightarrow q\bar{q}$ ($q = u, d, s$, or c) continuum events. We use two event-shape variables to distinguish the spherically symmetric $B\bar{B}$ events from the jet-like continuum events. A Fisher discriminant [16] is formed from 16 modified Fox-Wolfram moments [17] and the scalar sum of the transverse momenta. The second variable is the cosine of the angle between the B flight direction and the beam axis ($\cos \theta_B$) in the cms frame. For each variable, we obtain the corresponding signal and background probability density functions (PDFs) from large MC samples. A likelihood ratio $\mathcal{R}_{s/b} = \mathcal{L}_s / (\mathcal{L}_s + \mathcal{L}_b)$ is formed, where \mathcal{L}_s (\mathcal{L}_b) denotes the product of Fisher discriminant and $\cos \theta_B$ PDFs for the signal (background). The selection criteria on $\mathcal{R}_{s/b}$ are determined by maximizing the figure of merit, $N_S / \sqrt{N_S + N_B}$, where N_S (N_B) is the expected number of signal (continuum) events in the signal region. We require $\mathcal{R}_{s/b} > 0.65$, which removes 91% of the continuum while retaining 76% of the signal.

In addition to the dominant continuum background, various $B\bar{B}$ background sources are also studied. In the $B^0 \rightarrow \phi K_S^0 \gamma$ mode, some backgrounds from $b \rightarrow c$ decays, such as $D^0 \pi^0$, $D^0 \eta$ and $D^- \rho^+$ peak in the M_{bc} distribution. We remove the dominant peaking backgrounds by applying a veto to ϕK_S^0 combinations consistent with the nominal D mass [13]. Some of the charmless backgrounds, where the B meson decays to $\phi K^*(892)$, $\phi K \pi^0$ and $\phi K \eta$ also peak in M_{bc} . In these charmless modes, one of the photons from a π^0 or η may not be detected in the calorimeter while the other is reconstructed as the signal high-energy photon. Therefore, these backgrounds shift towards lower ΔE . Another significant background is non-resonant $B \rightarrow K^+ K^- K \gamma$, which peaks in the ΔE - M_{bc} signal region. The fraction of such events is estimated to be $(12.5 \pm 6.7)\%$ using the ϕ mass sideband, $1.05 \text{ GeV}/c^2 < M_{K^+ K^-} < 1.3 \text{ GeV}/c^2$, in data.

The signal yield is obtained from an extended unbinned maximum-likelihood fit to the two-dimensional ΔE - M_{bc} distribution in the fit region. We model the shape for the signal component using the product of a Crystal Ball line shape [18] for ΔE and a single Gaussian for M_{bc} . The continuum background is modeled with a product of first order Chebyshev polynomial for ΔE and an ARGUS [19] function for M_{bc} . The $b \rightarrow c$ background is modeled with a product of second order Chebyshev polynomial for ΔE and an ARGUS plus Gaussian function for M_{bc} . The small charmless backgrounds (except the non-resonant component) are modeled with a functional form that is the product of two Gaussians for ΔE and with a single Gaussian for M_{bc} [20]. In the final fit the continuum parameters are allowed to vary while all other background parameters are fixed to the values from MC simulation. The shape of the peaking backgrounds are fixed to that of signal in M_{bc} and ΔE . In the $B^+ \rightarrow \phi K^+ \gamma$ mode, the non-resonant background yield is fixed to the value from the ϕ sideband and assuming isospin symmetry, the same non-resonant fraction is used in the neutral mode. The signal shapes are adjusted for small differences between MC and data using a high statistics $B^0 \rightarrow K^*(892)^0 (\rightarrow K^+ \pi^-) \gamma$ control sample. The invariant mass of

the K^* candidates are required to satisfy $0.820 \text{ GeV}/c^2 < M_{K^+\pi^-} < 0.970 \text{ GeV}/c^2$. The fit yields a signal of $136 \pm 17 B^+ \rightarrow \phi K^+ \gamma$ and $35 \pm 8 B^0 \rightarrow \phi K_S^0 \gamma$ candidates. The projections of the fit results onto ΔE and M_{bc} are shown in Fig. 2. The signal significance is defined as $\sqrt{-2 \ln(\mathcal{L}_0/\mathcal{L}_{\max})}$, where \mathcal{L}_{\max} is the maximum likelihood for the best fit and \mathcal{L}_0 is the corresponding value with the signal yield fixed to zero. The additive sources of systematic uncertainty described below are included in the significance by varying each by its error and taking the lowest significance. The signal in the charged mode has a significance of 9.6σ , whereas that for the neutral mode is 5.4σ .

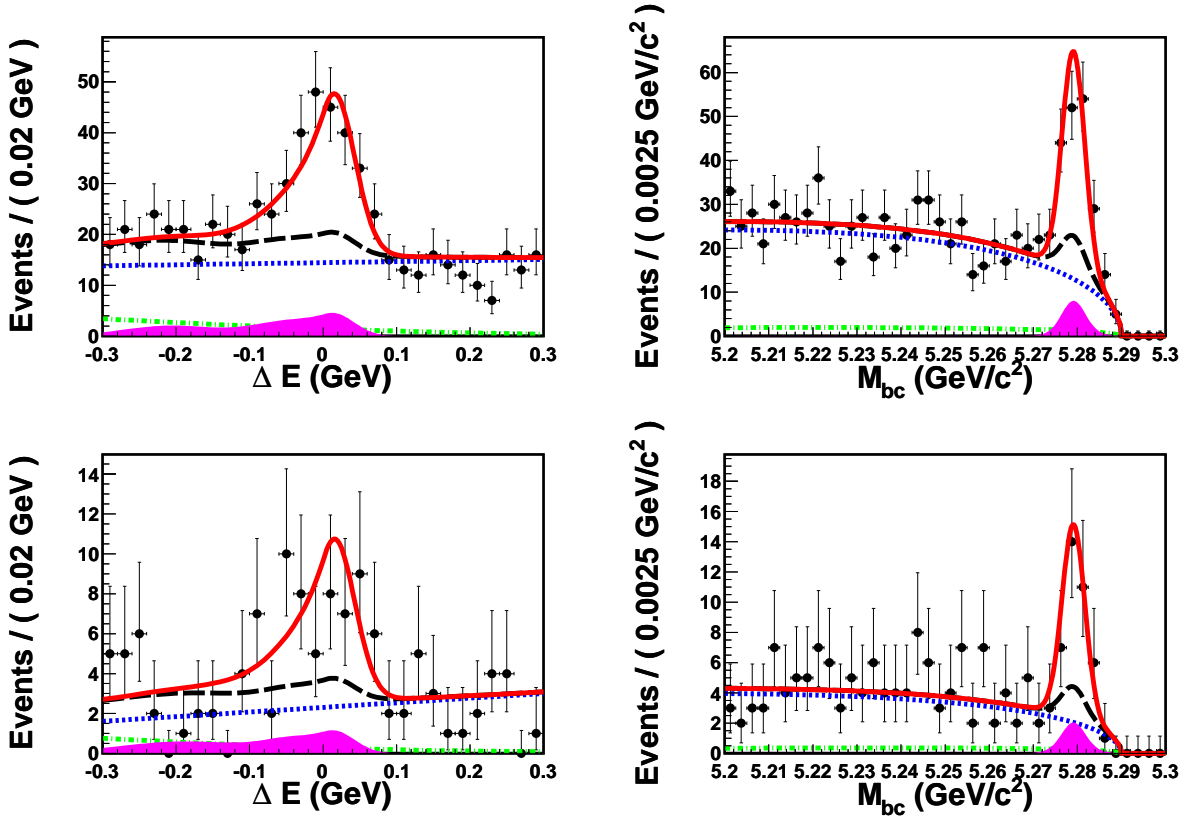


FIG. 2: The ΔE and M_{bc} projections for $B^+ \rightarrow \phi K^+ \gamma$ (upper) and $B^0 \rightarrow \phi K_S^0 \gamma$ (lower). The points with error bars represent the data. The different curves show the total fit function (solid red), total background function (long-dashed black), continuum component (dotted blue), the $b \rightarrow c$ component (dashed-dotted green) and the non-resonant component as well as other charmless backgrounds (filled magenta histogram).

We also examine the ϕK invariant mass distribution of the signal. To unfold the $M_{\phi K}$ distribution, we subtract all possible backgrounds and correct the ϕK invariant mass for the efficiency. The background-subtracted and efficiency-corrected $M_{\phi K}$ distributions are shown in Fig. 3. Nearly 72% of the signal events are concentrated in the low-mass region ($1.5 \text{ GeV}/c^2 < M_{\phi K} < 2.0 \text{ GeV}/c^2$). It is clear that the observed ϕK mass spectrum differs significantly from that expected in a three-body phase-space decay. The MC-determined reconstruction efficiencies (defined as the ratio of signal candidates passing all selection criteria to the total number of events generated) are corrected for this $M_{\phi K}$ dependence.

TABLE I: The signal yields, significances, weighted efficiencies and branching fractions for the $B^+ \rightarrow \phi K^+ \gamma$ and $B^0 \rightarrow \phi K^0 \gamma$ decay modes.

Decay mode	Yield	Significance (σ)	Efficiency (%)	Branching fraction (10^{-6})
$B^+ \rightarrow \phi K^+ \gamma$	136 ± 17	9.6	15.3 ± 0.1	$2.34 \pm 0.29 \pm 0.23$
$B^0 \rightarrow \phi K^0 \gamma$	35 ± 8	5.4	10.0 ± 0.1	$2.66 \pm 0.60 \pm 0.32$

From the signal yield (N_{sig}), we calculate the branching fraction (\mathcal{B}) as $N_{\text{sig}} / (\epsilon \times N_{B\bar{B}} \times \mathcal{B}_{\text{sec}})$, where ϵ is the weighted efficiency, $N_{B\bar{B}}$ is the number of $B\bar{B}$ pairs in the data sample, and \mathcal{B}_{sec} is the product of daughter branching fractions [13]. The results are summarized in Table I.

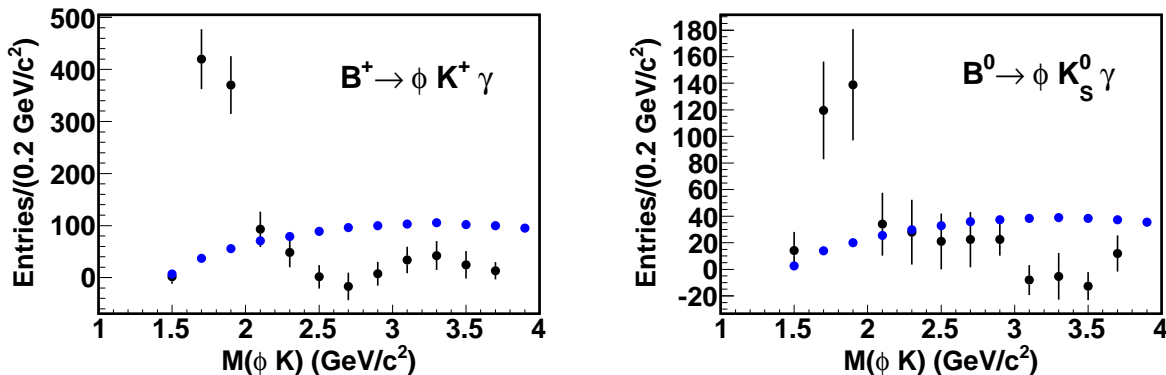


FIG. 3: The background-subtracted and efficiency-corrected ϕK mass distributions for $B^+ \rightarrow \phi K^+ \gamma$ (left) and $B^0 \rightarrow \phi K_S^0 \gamma$ (right). The points with error bars represent the data. The yield in each bin is obtained by the fitting procedure described in the text. The three-body phase-space model from the MC simulation is shown by the circles (blue) and normalized to the total data signal yield.

We fit the data with each fixed parameter varied by its $\pm 1 \sigma$ error, and then the quadratic sum of all differences from the nominal value is assigned as the systematic error on the signal yield. We checked for possible bias in the fitter by doing ensemble tests with MC pseudo-experiments. The statistical errors obtained from our measurements are within the expectations from the ensemble tests and a systematic error of 0.2% (2.7%) is assigned in the $B^+ \rightarrow \phi K^+ \gamma$ ($B^0 \rightarrow \phi K^0 \gamma$) mode. The largest contribution comes from the non-resonant yield (8.0%). The total systematic uncertainty assigned to the estimated yield is 8.2% (8.8%). We also assign a systematic error of 3.3% (4.6%) due to uncertainty on charged track efficiency, 1.4% due to particle identification, 2.4% due to photon detection efficiency, 1.4% due to uncertainty in the number of $B\bar{B}$ pairs in $B^+ \rightarrow \phi K^+ \gamma$ ($B^0 \rightarrow \phi K^0 \gamma$) mode. Furthermore, we assign a systematic error of 4.6% in the neutral mode due to K_S^0 reconstruction. The statistical uncertainty on the MC efficiency after reweighting is 0.9% (1.3%). The uncertainties due to daughter branching fractions account for a systematic contribution of 1.2%. We add each contribution above in quadrature to obtain the total systematic uncertainty of 9.9% (11.9%).

In summary, we report the first observation of radiative $B^0 \rightarrow \phi K^0 \gamma$ decays in Belle using a data sample of $772 \times 10^6 B\bar{B}$ pairs. The observed signal yield is 35 ± 8 with a significance of 5.4σ including systematic uncertainties. The measured branching fraction is $\mathcal{B}(B^0 \rightarrow \phi K^0 \gamma) = (2.66 \pm 0.60 \pm 0.32) \times 10^{-6}$. We also precisely measure $\mathcal{B}(B^+ \rightarrow \phi K^+ \gamma) = (2.34 \pm 0.29 \pm 0.23) \times 10^{-6}$ with a significance of 9.6σ . The signal events are mostly concentrated at low ϕK mass, which is similar to a two-body radiative decay. The neutral mode has enough statistics to measure time-dependent CP asymmetry in order to search for new physics from right-handed currents in radiative B decays.

We thank the KEKB group for the excellent operation of the accelerator, the KEK cryogenics group for the efficient operation of the solenoid, and the KEK computer group and the National Institute of Informatics for valuable computing and SINET3 network support. We acknowledge support from the Ministry of Education, Culture, Sports, Science, and Technology (MEXT) of Japan, the Japan Society for the Promotion of Science (JSPS), and the Tau-Lepton Physics Research Center of Nagoya University; the Australian Research Council and the Australian Department of Industry, Innovation, Science and Research; the National Natural Science Foundation of China under contract No. 10575109, 10775142, 10875115 and 10825524; the Department of Science and Technology of India; the BK21 and WCU program of the Ministry Education Science and Technology, the CHEP SRC program and Basic Research program (grant No. R01-2008-000-10477-0) of the Korea Science and Engineering Foundation, Korea Research Foundation (KRF-2008-313-C00177), and the Korea Institute of Science and Technology Information; the Polish Ministry of Science and Higher Education; the Ministry of Education and Science of the Russian Federation and the Russian Federal Agency for Atomic Energy; the Slovenian Research Agency; the Swiss National Science Foundation; the National Science Council and the Ministry of Education of Taiwan; and the U.S. Department of Energy. This work is supported by a Grant-in-Aid from MEXT for Science Research in a Priority Area ("New Development of Flavor Physics"), and from JSPS for Creative Scientific Research ("Evolution of Tau-lepton Physics").

* now at Okayama University, Okayama

- [1] E. Barberio *et al.*, Heavy Flavor Averaging Group (HFAG), arXiv:0808.1297.
- [2] M. Misiak *et al.*, Phys. Rev. Lett. **98**, 022002 (2007).
- [3] Throughout this paper, the inclusion of the charge-conjugate decay mode is implied unless otherwise stated.
- [4] D. Atwood, M. Gronau and A. Soni, Phys. Rev. Lett. **79**, 185 (1997).
- [5] D. Atwood, T. Gershon, M. Hazumi and A. Soni, Phys. Rev. D **71**, 076003 (2005).
- [6] V. D. Orlovsky, V. I. Shevchenko, Phys. Rev. D **77**, 093003 (2008).
- [7] D. Atwood, T. Gershon, M. Hazumi and A. Soni, hep-ph/0701021.
- [8] A. Drutskoy *et al.* (Belle Collaboration), Phys. Rev. Lett. **92**, 051801 (2004).
- [9] B. Aubert *et al.* (BaBar Collaboration), Phys. Rev. D **75**, 051102 (2007).
- [10] S. Kurokawa and E. Kikutani, Nucl. Instrum. Methods Phys. Res., Sect. A **499**, 1 (2003), and other papers included in this volume.
- [11] A. Abashian *et al.* (Belle Collaboration), Nucl. Instrum. Methods Phys. Res., Sect. A **479**, 117 (2002).
- [12] We use the EvtGen B meson decay generator, D. J. Lange, Nucl. Instrum. Methods Phys. Res., Sect. A **462**, 152 (2001). The detector response is simulated with GEANT, R. Brun *et*

- al.*, GEANT 3.21, CERN Report DD/EE/84-1 (1984).
- [13] C. Amsler, *et al.*, Physics Letters **B 667**, 1 (2008).
 - [14] K-F. Chen *et al.* (Belle Collaboration), Phys. Rev. D **72**, 012004 (2005).
 - [15] P. Koppenburg *et al.* (Belle Collaboration), Phys. Rev. Lett. **93**, 061803 (2004).
 - [16] R. A. Fisher, Annals of Eugenics **7**, 179 (1936).
 - [17] The Fox-Wolfram moments were introduced in G. C. Fox and S. Wolfram, Phys. Rev. Lett. **41**, 1581 (1978). The modified Fox-Wolfram moments used in this analysis are described in S. H. Lee *et al.* (Belle Collaboration), Phys. Rev. Lett. **91**, 261801 (2003).
 - [18] T. Skwarnicki, Ph.D. thesis, Institute for Nuclear Physics, Krakow, 1986; DESY Internal Report No. DESY F31-86-02, 1986. The function is widely used to describe asymmetric distributions caused by shower leakage in crystal calorimeters.
 - [19] H. Albrecht *et al.* (ARGUS Collaboration), Phys. Lett. B **241**, 278 (1990).
 - [20] $f(\Delta E, M_{bc}) = G_1(\Delta E - E_1) G(M_{bc} - M_0) + G_2(\Delta E - E_2) G(M_{bc} - M_0)$, where G_1 , G_2 and G_3 are Gaussian functions and E_1 , E_2 and M_0 are constants.